© 2014. Published by The Company of Biologists Ltd | The Journal of Experimental Biology (2014) 217, 3095-3107 doi:10.1242/jeb.092742

RESEARCH ARTICLE

Analyses of the mouthpart kinematics in *Periplaneta americana* (Blattodea, Blattidae) using synchrotron-based X-ray cineradiography

Christian Schmitt‡, Alexander Rack*,‡ and Oliver Betz

ABSTRACT

The kinematics of the biting and chewing mouthparts of insects is a complex interaction of various components forming multiple jointed chains. The non-invasive technique of *in vivo* cineradiography by means of synchrotron radiation was employed to elucidate the motion cycles of the mouthparts in the cockroach *Periplaneta americana*. Digital X-ray footage sequences were used in order to calculate pre-defined angles and distances, each representing characteristic aspects of the movement pattern. We were able to analyze the interactions of the mouthpart components and to generate a functional model of maxillary movement by integrating kinematic results, morphological dissections and fluorescence microscopy. During the opening and closing cycles, which take about 450–500 ms on average, we found strong correlations between the measured maxillary and mandibular angles, indicating a strong neural coordination of these movements. This is manifested by strong antiphasic courses of the maxillae and the mandibles, antiphasic patterns of the rotation of the cardo about its basic articulation at the head and by the deflection between the cardo and stipes. In our functional model of the maxilla, its movement pattern is explained by the antagonistic activity of four adductor-promotor muscles and two abductor-remotor muscles. However, beyond the observed intersegmental and bilateral stereotypy, certain amounts of variation across subsequent cycles within a sequence were observed with respect to the degree of correlation between the various mouthparts, the maximum, minimum and time course of the angular movements. Although generally correlated with the movement pattern of the mandibles and the maxillary cardo-stipes complex, such plastic behaviour was especially observed in the maxillary palpi and the labium.

KEY WORDS: Biomechanics, Cineradiography, Functional morphology, Feeding, Imaging, Insecta, Kinematics, Maxilla, Morphology, Mouthparts, *Periplaneta americana*, Resilin, Synchrotron radiation

INTRODUCTION

Although the principal morphology of insect mouthparts has been studied for a number of orders, only a few observational studies have elucidated their function during feeding. Studies of the biting and chewing mouthparts have been conducted, for instance, on cockroaches (Blattodea) (Popham, 1961), earwigs (Dermaptera) (Popham, 1959) and carabids (Coleoptera) (Evans, 1964; Forsythe, 1982; Forsythe, 1983; Evans and Forsythe, 1985). However, these studies are exclusively based on qualitative approaches and do not present quantifiable analyses on the coordination and kinematics of the various mouthparts over time. The aim of this study was to focus on the kinematics of biting and chewing mouthparts using *Periplaneta americana* (Linnaeus 1758) as an example. Previous studies have shown that the movement of such mouthparts is rhythmic and highly coordinated (Smith, 1985; Popham, 1959; Popham, 1961). Research on locusts (Seath, 1977a; Seath, 1977b; Rast and Bräunig, 2001a; Rast and Bräunig, 2001b) has demonstrated the motor neural correlations of such a stereotyped pattern at the level of the subesophageal ganglion (SOG). The SOG, for its part, is modulated by the frontal ganglion and the ventral nerve chord (Blaney and Simmonds, 1987; Griss, 1990; Griss et al., 1991; reviewed in Chapman, 1995a). In arthropods, almost all the chemo- and mechanoreceptors associated with ingestion and the motor neurons of the mandibular muscles project onto this ganglion (Altman and Kien, 1979; Kent and Hildebrand, 1987; Chapman, 1995b).

As in walking, the varying demands of load during feeding must be met by variation in the velocity, force and frequency of muscle contractions, thereby implying modulation by sensory information (Smith, 1985). As an example, Seath (Seath, 1977a; Seath, 1977b) describes a context-sensitive precision control of the mandibles of locusts via sensory modulated muscle action governed by resistance reflexes.

Despite these neurobiological findings, descriptive and experimental studies of mouthpart feeding coordination and kinematics in insects are scarce (cf. Seath, 1977a; Seath, 1977b; but this study does not consider the maxillae). This is because the detailed kinematics of all the elements of the mouthparts cannot be recorded simultaneously to date, because their overlapping positions and complex motion has limited any kind of image analysis.

In this regard, the technique of *in vivo* high-speed X-ray imaging (Westneat et al., 2003; Socha et al., 2007; Westneat et al., 2008; Betz et al., 2008; Schmitt et al., 2009; Rack et al., 2010) enables the display of overlapping structures in the interior of living animals with high temporal resolution and thus reveals the function of internal organ systems. For X-ray cineradiography, synchrotron light sources generate a photon beam that (1) propagates quasi-parallel, (2) has fluxes that are by orders of magnitude higher than laboratory sources and (3) allows the exploitation of more sophisticated contrast modalities (Betz et al., 2008). The use of synchrotron radiation is thus the next step in fast-imaging development, i.e. high-speed hard X-ray cineradiography employing phase contrast mechanisms (Westneat et al., 2003; Westneat et al., 2008).

Eberhard Karls Universität Tübingen, Institut für Evolution und Ökologie, Professur für Evolutionsbiologie der Invertebraten, Auf der Morgenstelle 28, D-72076 Tübingen, Germany.
*Present address: European Synchrotron Radiation Facility (ESRF), 6 Rue Jules Horowitz, 38000 Grenoble, Cedex, France.

‡Authors for correspondence (christian.schmitt@uni-tuebingen.de; alexander.rack@esrf.fr)

Received 27 June 2013; Accepted 3 June 2014

List of abbreviations

ANKA	Angströmquelle Karlsruhe
CC	correlation coefficient
CV	coefficient of variation
fps	frames per second
ga	galea
KIT	Karlsruhe Institute of Technology
lc	lacinia
lmt	laminatentorium
m	membranous surface area of stipes
M	Musculus
PC	principal component
PCA	principal component analysis
pm	palpus maxillaris/maxillary palp
R|L	right|left
s.d.	standard deviation
SEM	scanning electron microscopy
SOG	subesophageal ganglion

In the present contribution, we use synchrotron-based X-ray cineradiography with a temporal resolution of up to 125 frames per second (fps) to describe and quantify the kinematics of the various mouthparts and their interactions in *P. americana*. The aim of this study is to use this data (together with our investigation of the maxillary muscles) to generate a functional model of the maxilla in order to understand its complex kinematics. Our hypotheses to be tested in this study can be developed as follows. (1) Owing to the common neuronal control of the various mouthpart components by the SOG and owing to the organization of these components within a complex functional unit, we expect both a high degree of rhythmicity and a strong synchronicity in the movement of the different mouthpart components. The synchronicity serves as a measure of the stereotypic coupling of the mouthpart components, whereas the rhythmicity of the individual movements indicates a continuous and uniform movement sequence. (2) Within the framework of the complex motion cycle of the mouthparts, we expect differences concerning the degree of synchronization of certain parts of the mouthpart complex. We expect a pronounced synchronicity for the movement of corresponding mouthpart components of both sides of the body (i.e. the maxillae and mandibles of the left and right side, respectively) as well as of the basal elements (cardo and stipes) of the maxilla. The movement of these components have to be functionally coupled to ensure the efficient manipulation and subsequent ingestion of food. In contrast, some mouthpart components (e.g. the maxillary palps and the labium) have to be used in a more flexible manner during food uptake, so it is likely that their movements are modulated to a higher extent and consequently exhibit a lesser degree of synchronicity.

RESULTS

Mouthpart kinematics

Our cineradiographic movies revealed a rhythmic, symmetrical and synchronous movement pattern of the mouthparts, whereupon the maxillae ran in antiphase with respect to the mandibles (cf. supplementary material Movies 1 and 2). Digitizing pre-defined mouthparts over the course of several movement cycles made it possible to quantify this pattern using different approaches.

Correlation analyses

Mandibles

In almost all analyzed sequences, both mandibles perform regular opening and closing movements about their basic articulation at the head capsule during feeding on soft food material (cf. Fig. 1). No obvious differences between the time spans needed for opening and closing of the mandibles were observed. Fig. 1A shows representative footage depicting one motion cycle of the mandibles (approximately 500 ms). The angle versus time diagram (Fig. 1B) shows the sequence of both the opening angle and the gap width of the mandibles for the movement cycle depicted in this sequence (Fig. 1A). The patterns of both angles (left and right mandible) are sinusoidal and correspond in terms of both their amplitude and duration with each other (Fig. 1C). There is hardly any variation in the maximum (60–65 deg) and minimum (42 deg) values of the opening angle within this sequence. Accordingly, the peaks for the gap width of the mandibles are similarly invariable during the maximally opened state (approximately 750 µm) and the maximally closed state (approximately −300 µm). The obtained negative value is attributable to the tips of the mandibles overlapping, i.e. exceeding the zero line during the closing movement (cf. Fig. 1B,C). The value for the distance between the tips of the mandibles consequently increases as the tips start to cross each other. To obtain a better overview, these distances are indicated by negative values.

Overall, both the mandibular angle *m* (cf. Fig. 9B) and the ‘gap width of mandibles’ show a high consistency of their kinematics during opening and closing in all the analyzed movies [given are the grand means of the maxima (minima in brackets) for N=12]: *m* right side: 60.0 deg (40.8 deg), standard deviation (s.d.): 5.8 (5.0); *m* left side: 58.5 deg (43.1 deg), s.d.: 4.3 (4.5); ‘gap width of mandibles’: 741 µm (−158 µm), s.d.: 263.6 (148.5). The same applies to the time necessary for the completion of an entire motion cycle of the mandibles, i.e. the time between two maxima in the angle versus time diagrams (*m* right side: 451 ms, s.d.: 105.3; *m* left side: 498 ms, s.d.: 123.9).

Maxillae

As for the mandibles, our statistical analyses revealed a uniformly occurring rhythmic movement of the maxillae that appeared bilaterally coupled (including the ab- and adduction of the maxillary palpus at its base via angle *e* in Fig. 10C). This coordination was indicated by the maxillary angles *a* and *d* (cf. Fig. 10) being highly consistent with respect to their kinematics during opening and closing across all the analyzed movies [given are the grand means of the maxima (minima in brackets) for N=12]: *a* right side: 159 deg (139 deg), s.d.: 15.1 (8.1); *a* left side: 163 deg (142 deg), s.d.: 12.5 (11.3); *d* right side: 106 deg (83 deg), s.d.: 8.1 (10.5); *d* left side: 105 deg (81 deg), s.d.: 12.6 (12.5). The same applies to the time necessary for the completion of an entire motion cycle of the maxillae, i.e. the time between two maxima in the angle versus time diagrams (*a* right side: 446 ms, s.d.: 113.7; *a* left side: 447 ms, s.d.: 128.7; *d* right side: 455 ms, s.d.: 119.7; *d* left side: 446 ms, s.d.: 121.1).

If the maxillary angles are added to the sequence depicted in Fig. 1, the strong synchronization between the right and the left side of the body is further confirmed (Fig. 2A,B,D; Fig. 3). This is a general pattern that applies to all the analyzed sequences. In contrast, the angles describing the kinematics of the maxillary palps are less synchronized regarding both sides of the body (Fig. 2C, Fig. 3). Almost all the maxillary angles are highly intercorrelated with respect to their amplitude and duration. This also applies to their correlation with the opening angle of the mandibles (Fig. 2A,D; Fig. 3). In Fig. 3, the correlation tables for all the sequences are summarized to provide an overview of the inter-individual consistence of the correlations within the mouthpart system. Strong correlations exist between the opening angles of the mandibles (angles *m*) and both maxillae (angles *a*). A strong synchronization

The Journal of Experimental Biology (2014) doi:10.1242/jeb.092742

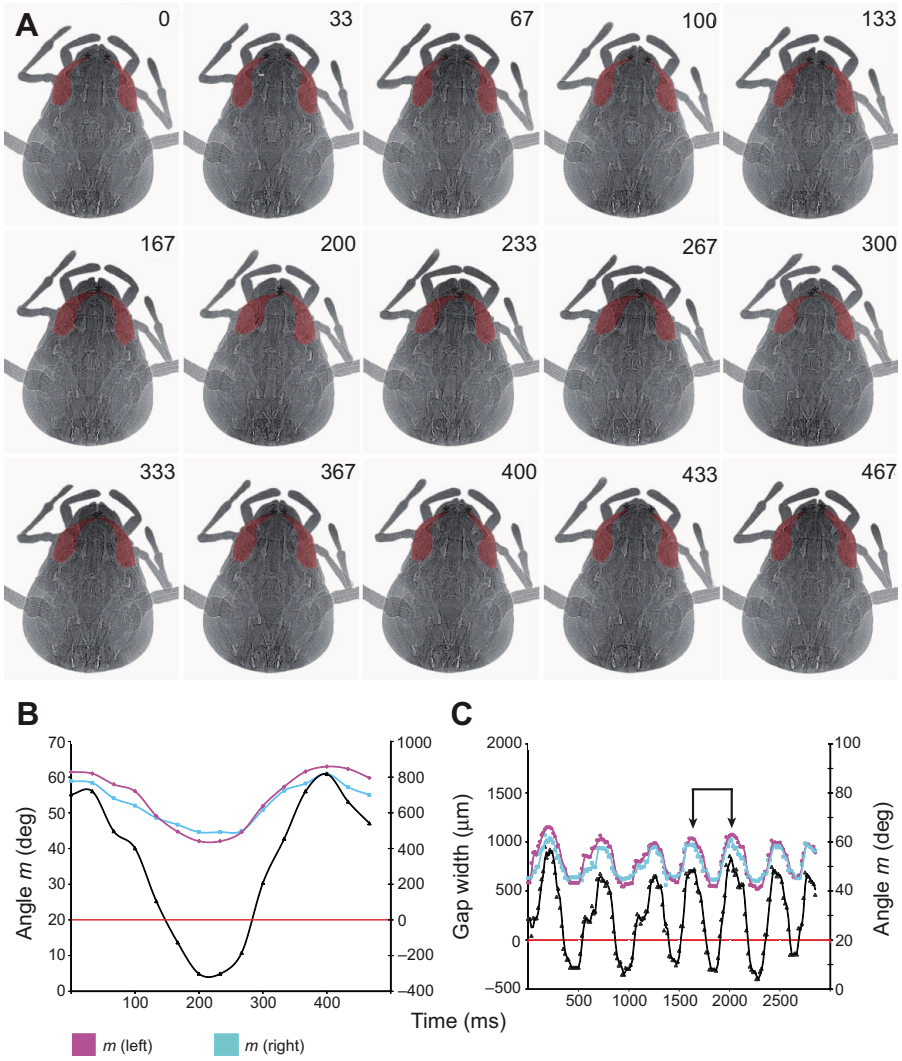

Fig. 1. Kinematics of the mandibles during the feeding process. (A) Representative radiography image sequence (*Periplaneta*_4) of approximately 500 ms depicting the opening and closing cycle of the mandibles (red). The numbers indicate the time course of the depicted sequence (ms that elapsed from the start). (B) Angle versus time diagram of the angle *m* and distance versus time diagram of the gap width of the mandibles (black line) within the image sequence shown in A. (C) Angle versus time diagram and pattern of the gap width depicting the complete movie sequence (bracket with arrow tips indicates the motion cycle displayed in A and B; horizontal red line in B and C indicates the condition when the gap width of the mandibles (black line) is zero (further closing of the mandibles leads to negative values of the gap width, because their tips are overlapping). For an explanation of angle *m* and gap width of mandibles, see Fig. 9B.

between the mandibles and the maxillae can be found for almost all of the 12 analyzed sequences [e.g. mandibular opening angle *m* (left and right) with the maxillary angles *a* in Fig. 3]. The movement of the maxillary palps (angles *e* and *f*) are, in most cases, correlated only to a low or medium extent with the general maxillary, mandibular and labial movements (Fig. 3).

Labium

During feeding the labium performs regular pro- and retraction movements (Fig. 2D) [grand means of the duration of an entire cycle: 568 ms (s.d.: 269.2), N=12]. Its maximum protraction distance (as measured relative to its most retracted condition in a specimen) amounts to a grand mean of 334 µm (s.d.: 127.5, N=12). In many cases, changes in the angles of the mandibles and the maxillae are only weakly correlated with the pro- and retraction of the labium (Fig. 3). These correlations can be both negative and positive indicating certain flexibility, probably depending on the current feeding situation.

Coefficients of variation

The coefficients of variation (CVs) of the maxima, the minima and the time spans presented in the previous section are an additional clue with regard to the variability of the kinematics of the individual mouthpart elements, whereby the CVs are only comparable within a particular unit, i.e. the angle, distance or time measurements. The medians and the interquartile ranges of the boxplots reveal that the movement angles of the elements of the mandibles and the maxillae are constant, showing CVs of approximately ≤10% (medians) (Fig. 4A,B). In some cases, as indicated by the longer whiskers in individual boxplots, single cycles within a specimen might largely deviate from the general pattern, leading to higher CVs and indicating a certain amount of (context-dependent) flexibility, even in the movements of the mandibles and the cardo-stipes complex of the maxilla. With regard to the time span needed for one motion cycle, the strong coordination between the mandibles and the maxillae is confirmed by the similarity of their medians (Fig. 4C). The labium appears more plastic in both its pro- and retraction time and its protrusion distance (Fig. 4A–C).

Principal component analyses

The high coordination of the individual elements of the mouthparts was also confirmed by the principal component analyses (PCA) (Tables 1, 2). In five specimens, there were extracted three and four PCs, explaining 81.8–89.7% (three PCs) and 86.7–91.0% (four extracted PCs) of the total variance, respectively. In two specimens, only two PCs were extracted, explaining 81% of the total variance. Our analyses confirmed that the maxillary angle *d* between cardo and stipes was generally loaded on PC1 or PC2 in an opposite way

The Journal of Experimental Biology (2014) doi:10.1242/jeb.092742

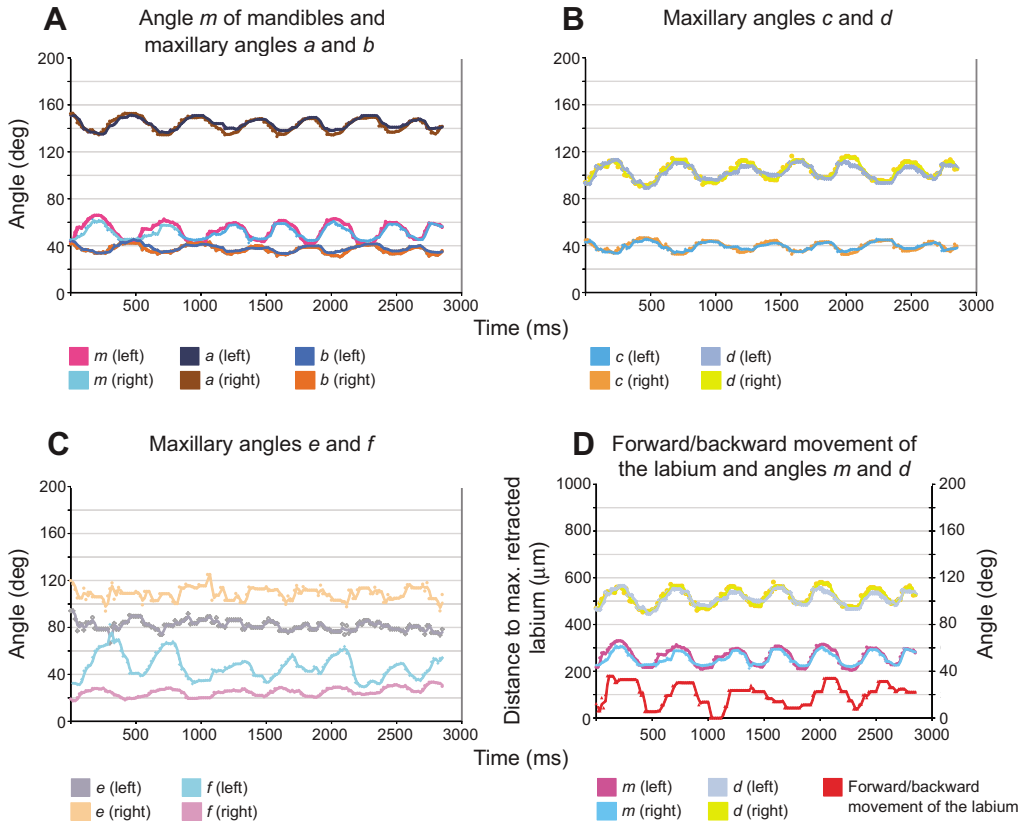

Fig. 2. Representative angle versus time diagrams of approximately 3000 ms depicting the relationships between the opening angle of the mandibles *m*, the maxillary angles *a–f* and the pro- and retraction movement of the labium. For an explanation of angles *m* and *a–f*, see Figs 9, 10.

from all the other angles of the maxillary body (i.e. *a*, *b* and *c*). At the same time, the sign of the loading of this angle on the PCs corresponded consistently with the mandibular angle *m* and the corresponding mandibular 'gap width' (e.g. Table 2). The loadings of the variables on the PCs further confirmed the close correspondence of the mouthpart elements of both the left and the

	m (right)	*m* (left)	Gap w.	*a* (right)	*a* (left)	*b* (right)	*b* (left)	*c* (right)	*c* (left)	*d* (right)	*d* (left)	*e* (right)	*e* (left)	*f* (right)	*f* (left)	Labium
m (right)		9	12	-9 | 3	-10 | 1	-8 | 3	-10 | 1	-11	-9	-3 | 9	-1 | 10	-5 | 4	-5 | 5	-1 | 8	-3 | 8	-2 | 9
m (left)	**0.82**		12	-11 | 1	-10 | 1	-10 | 1	-8 | 3	-12	-9	-1 | 11	-2 | 9	-8 | 2	-8 | 3	-2 | 9	-1 | 10	-2 | 7
Gap w.	**0.82**	**0.83**		-11 | 1	-9 | 1	-11 | 1	-10	-11	-10	11	10	-6 | 3	-7 | 3	-1 | 9	-2 | 9	-1 | 8
a (right)	-0.38	**-0.75**	-0.54		12	11	-1 | 10	12	11	-12	-10	-1 | 9	-1 | 9	-9 | 1	-8 | 2	-7 | 2
a (left)	**-0.73**	-0.56	-0.68	**0.77**		11	12	11	12	-12	-12	-2 | 9	-2 | 10	-11	-6 | 3	-9 | 3
b (right)	-0.38	-0.60	-0.30	**0.82**	0.62		11	-1 | 11	12	-11 | 1	-12	11	-1 | 10	-7 | 2	-8 | 3	-6 | 2
b (left)	-0.49	-0.30	-0.39	**0.72**	**0.83**	**0.77**		-2 | 10	12	-10 | 1	-12	-1 | 9	11	-9 | 1	-7 | 4	-8 | 3
c (right)	-0.37	-0.55	-0.45	**0.90**	**0.76**	0.66	0.63		-1 | 10	-12	-10 | 1	-2 | 8	-1 | 10	-9	-8 | 2	-7 | 2
c (left)	-0.46	-0.61	-0.51	**0.79**	**0.85**	0.63	**0.73**	**0.80**		-11 | 1	-12	-1 | 9	10	-7 | 1	-7 | 1	-6 | 5
d (right)	0.34	0.67	0.57	**-0.96**	**-0.77**	**-0.92**	**-0.84**	**-0.96**	**-0.79**		-1 | 10	-10 | 2	-10 | 2	-1 | 8	-2 | 9	-2 | 8
d (left)	0.52	0.46	0.53	**-0.81**	**-0.94**	**-0.74**	**-0.92**	**-0.76**	**-0.96**	**0.87**		-10 | 1	-11	9	-3 | 8	-3 | 7
e (right)	-0.37	-0.37	-0.26	0.48	0.35	0.57	0.48	0.41	0.58	-0.38	-0.44		11	-4 | 6	-7 | 2	-4 | 5
e (left)	-0.13	-0.29	-0.21	0.44	0.40	0.60	0.63	0.41	0.57	-0.51	-0.63	**0.76**		-4 | 5	-8 | 3	-4 | 5
f (right)	0.58	0.40	0.35	-0.40	-0.35	-0.28	-0.25	-0.38	-0.31	0.31	0.22	0.22	0.18		-3 | 5	-4 | 5
f (left)	0.62	0.53	0.52	-0.35	-0.42	-0.25	-0.36	-0.34	-0.24	0.30	0.28	-0.42	-0.34	0.35		-2 | 6
Labium	0.45	0.46	0.37	-0.39	-0.34	-0.39	-0.36	-0.36	-0.22	0.37	0.33	0.21	0.28	0.18	0.46	

Fig. 3. Summary of the correlation analyses. Upper half of the figure: summary of the correlation analyses (according to Pearson) of all parameters (angles: mandibles, maxillae; distances: gap width of mandibles, labium) of all 12 specimens. All correlations (negative and positive) with significance ≤0.05 are counted and listed (negative|positive). Bottom half of the figure: medians of the correlation coefficients (CCs). High CCs (bold numbers represent high or very high coordination as defined in Materials and methods) represent a strong stereotypy in the movement of two mouthpart elements, whereas a missing or weak CC is indicative of a high modulation capacity. Pronounced synchronicities can be stated for the movements of corresponding mouthparts regarding both body sides (i.e. angles *m*, *a*, *b*, *c*, *d*, and *e* of the left and right side of the body, respectively), as well as for the movement patterns of the basal elements (cardo and stipes) of the maxillae. The same applies for the correlation of the movement of the mandibles with that of the maxillae about their articulations at the head capsule (angles *m* and *a*). A higher degree of modulation is indicated by weaker CCs within the movement of the labium with that of the mandibles and the maxillae, respectively. Gap w., gap width.

The Journal of Experimental Biology (2014) doi:10.1242/jeb.092742

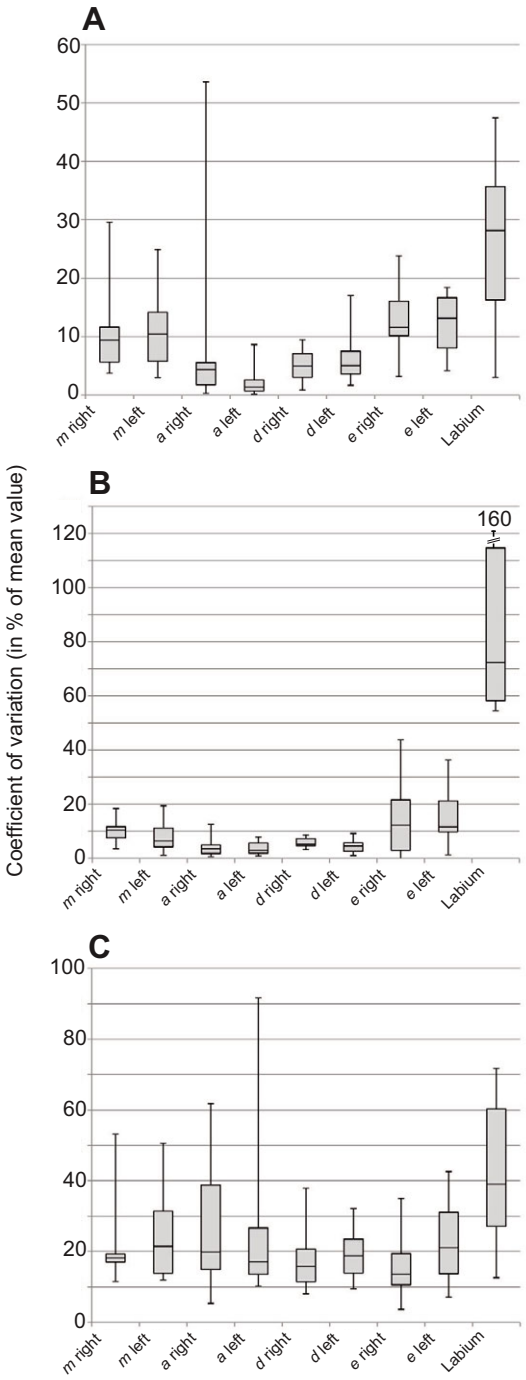

Fig. 4. Variation of the kinematics of the observed mouthparts. Boxplot diagrams of the coefficients of variation of the (A) maxima, (B) minima and (C) time spans needed for an entire motion cycle (i.e. opening and closing) of the parameters used to describe the mouthpart kinematics (cf. Figs 9, 10). Boxes represent interquartile range, lines represent medians and the whiskers represent the range.

right side, although in six cases (in which three or more, often four, PCs were extracted), the corresponding left and right elements might have been loaded onto different PCs. Both the angles of the maxillary body and the mandibles, usually, were highly loaded on PC1, further supporting the strong synchronization of these mouthpart elements. Only in three specimens were the mandibles loaded onto PC2. The loading pattern of the angles of the maxillary palpus (i.e. angles *e* and *f*) indicated a behaviour that was more independent from the maxillary body. In only five specimens was the angle *e* (basal articulation of the palpus at the stipes) loaded together with the other maxillary angles on PC1, and angle *f* did so only once. In all the other specimens, these angles were loaded on higher PCs. The movement of the labium did not consistently load with the other mouthpart elements. In five sequences, it loaded together with the maxillary and mandibular angles on PC1, whereas in five other sequences, it was separately loaded on a higher PC, explaining less of the total variance.

Table 1. Results of a PCA performed on the sequence *Periplaneta_4*

Component	Eigenvalue	Explained variance (%)	Cumulated explained variance (%)
PC1	9.69	60.55	60.55
PC2	3.41	21.30	81.85

List of the extracted principle components (PC1 and 2) and their explained variances.

Autocorrelation analysis

This analysis was exemplarily conducted for one representative individual (*Periplaneta*_4) (cf. supplementary material Fig. S1A–H). It confirmed the high rhythmicity already demonstrated in our angle versus time diagrams (Figs 1, 2). There appear significances of alternating positive and negative autocorrelation coefficients that re-occur on a regular basis with respect to the progressing lag time. This is indicative of the motion cycles of most mouthpart elements following a sinusoidal pattern (supplementary material Fig. S1). In this sequence, almost all the angles follow this regular pattern, whereas lower or lacking autocorrelations were determined for the general movement of the maxillary palpus about its insertion at the palpifer (cf. angle *e* in Fig. 10C and supplementary material Fig. S1F).

Functional model of the maxillary kinematics

The observed pro- and retraction of the maxilla during a motion cycle is paralleled by the ad- and abduction of its tips (i.e. the galea–lacinia complex). Such a motion cycle involves strong flexion and extension movements in the cardo-stipes articulation accompanied by the in- and outward rotation of the cardo around its

Table 2. Loadings of the kinematic variables (angles of mandibles and maxillae, distances of labium and gap width of mandibles) on the two extracted principal components of the sequence *Periplaneta_4*

	Principal component 1	Principal component 2
a left	0.95	
d left	−0.93	
c left	0.93	
c right	0.91	
gap width	−0.89	
d right	−0.89	
m right	−0.89	
a right	0.88	
m left	−0.88	
b left	0.86	
b right	0.79	
f left	−0.68	
e left	0.50	
labium		0.79
e right		−0.78
f right		0.70

For an explanation of the variables, see Figs 9 and 10.

The Journal of Experimental Biology (2014) doi:10.1242/jeb.092742

Table 3. List of the most important muscles (nomenclature according to Kéler, 1963) powering the maxillary movement, illustrating their points of insertion as confirmed by our dissections and their proposed function (the latter according to Kéler, 1963)

Name	Insertion	Function
M. craniocardinalis externus (M15)	At dumbbell-shaped structure of saddle joint of cardo	Rotator, retracting maxilla by abduction of cardo
M. tentoriocardinalis (M17)	Endoskeleton margin, parallel to cardinostipital fissure	Promotor, protracting maxilla by adduction of cardo
M. tentoriostipitalis (M18)	At medial aspect of the stipes	Adductor, pulls stipes mediad toward hypopharynx
M. craniolacinialis (M19)	Medial, basal edge of the lacinia	Adductor of lacinia
M. stipitolacinialis (M20)	At basal margin of lacinia, next to M19	Adductor of lacinia
M. stipitogalealis (M21)	At basal margin of galea, lateral wall	Abductor of galea

The muscles responsible for the kinematics of the maxillary palps and the palpomeres are not listed. M, musculus.

articulation with the head capsule (Fig. 6; supplementary material Movies 1, 2). To generate a functional model of the maxillary kinematics from our footage, we investigated the maxillary muscle complex (Table 3). The most important muscles that power the maxillary movement are shown in Fig. 5 together with their functions as presumed from the literature (Kéler, 1963; Snodgrass, 1993). The insertion points of these muscles in *P. americana* could be confirmed by our direct dissections of the maxillae.

The functional model explaining the observed maxillary kinematics consists of four consecutive phases (Fig. 6).

Phases of the maxillary motion cycle

First phase of the motion cycle

Both the cardo and the stipes are maximally protracted, and the cardo is kept maximally adducted with respect to the medial line [(1) in Fig. 6B]. This is reflected in the maxillary angle *d*, which describes the cardo–stipes articulation, assuming its maximum of ca. 110 deg (Fig. 6A) and the maxillary angle *a* reaching its minimum of 135 deg. The protraction of the maxilla is effected by the contraction of the M17, although we assume that the involved increase of the angle *d* is facilitated by non-muscular preflex movements caused by the protein resilin embedded into the articulation membrane (see next section). Moreover, the widening of the angle *d* might be passively caused by the adduction pressure that both abutting maxillary galeae exert on each other.

The continuing adduction of the apical part of the maxilla toward the medial line is caused mainly by the simultaneous contraction of the M18. During this process, both tips of the maxillae (i.e. the galeae) are still kept in contact and finally reach their maximally protracted position. At the end of phase 1, the cardo is kept maximally adducted, both the cardo and the stipes are maximally stretched forward, and the maxillary palp (angle *e*) is maximally retracted.

Second phase of the motion cycle

The retraction of the maxilla is initiated as reflected by the maxillary angle *d* starting to decrease, while the maxillary angle *a* increases [(2) in Fig. 6B]. This is reflected in the tip of the maxilla moving laterad away from the medial line, as caused by the action of the M15. The actual retraction of the maxilla is enabled by the flexion of the stipes with respect to the cardo. The flexion is made possible by the action of the M19. The maxillary palps start re-moving to the anterior.

Third phase of the motion cycle

In this third phase [(3) in Fig. 6B], both the retraction and the abduction of the maxilla away from the medial line are complete. As a consequence, the cardo and the stipes are maximally bent against each other, so that the maxillary angle *d* attains its minimum. In this way, the resilin-containing arthrodial membrane between the cardo and stipes is compressed and loaded for its rebound in the next phase (phase 4) of the motion cycle.

In this phase of the motion cycle, the angle *a* displays its maximum, which is associated with a maximum abduction of the cardo and a pronounced retraction of the maxilla. The described movements can be explained by the complete contraction of both the M15 and M19, whereas the M17 and M18 are completely relaxed. Both maxillary palps are maximally stretched forward in relation to the stipes.

Fourth phase of the motion cycle

The re-protraction and re-adduction of the maxilla is initiated [(4) in Fig. 6B]. Although probably initialized by the elastic rebound of resilin, the protraction of the maxilla is increasingly effected by muscular contraction, probably passively supported by the abutting of both galeae at the medial line of the body. At the beginning of this phase, both the M15 and the M19 are relaxing, and the maxilla is rotated inward by the contraction of the M17. At the same time, the contraction of the M18 causes the adduction of the stipes toward the midline. As a result, the tips of the maxillae (i.e. the galeae) of both sides medially contact each other, while being further protracted; they reach their maximum protraction in the subsequent (first) phase of the motion cycle [(1) in Fig. 6B].

Fluorescence microscopy of the maxillae

Intense blueish autofluorescence (indicating the presence of resilin) was found, especially on the membranous components, i.e. less sclerotized cuticular surfaces and the joint structures (e.g. the joint between the cardo and stipes). Fig. 7 depicts the membranous

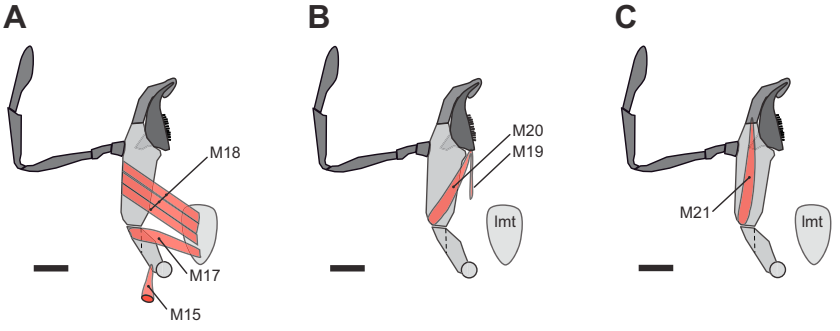

Fig. 5. Model of the maxilla highlighting the muscles (red) listed in Table 3. (A) M. craniocardinalis externus (M15), M. tentoriocardinalis (M17), M. tentoriostipitalis (M18); (B) M. craniolacinialis (M19), M. stipitolacinialis (M20); (C) M. stipitogalealis (M21). lmt, laminatentorium; M, Musculus. Scale bars: 1 mm.

The Journal of Experimental Biology (2014) doi:10.1242/jeb.092742

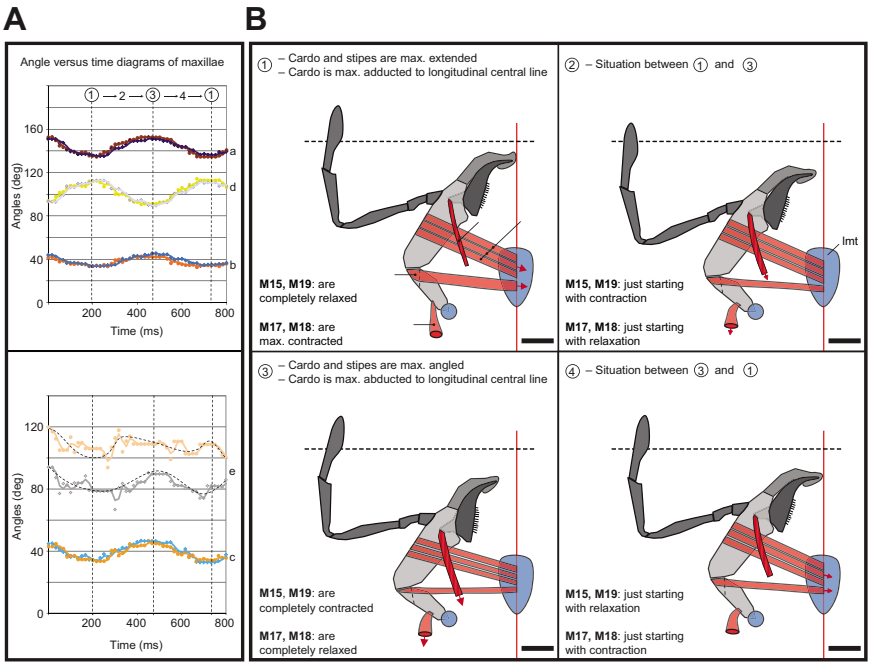

Fig. 6. Functional model explaining the observed motion cycle of the maxilla during a time frame of 800 ms. The sequence is divided into four consecutive segments (first to fourth phase of motion cycle). (A) Angle versus time diagrams as observed from a representative movie. (B) Positions of the individual maxillary elements and the assumed corresponding activity of the involved muscles. Because the action of the respective muscles could not be observed directly, their effect on the complex maxillary movement pattern had to be indirectly re-constructed via the changes of the angles determined in the cineradiographic analysis. For the positions of the triangles, by which the maxillary angles *a* to *e* were constructed, see Fig 9C–E and Fig 10. For description of muscles, see Table 3 and Fig. 5. Structures highlighted in blue are fixed structures within the tentorium or the head capsule. lmt, laminatentorium. Scale bars: 1 mm.

integument between the insertion of the maxillary palp and the joint region between the cardo and stipes of the right maxilla as seen from the dorsum. There appears a gradient of the resilin distribution between the soft integument (featuring a strong autofluorescence) and stronger sclerotized areas (sclerites).

DISCUSSION

Our analysis shows that synchrotron *in vivo* cineradiography (e.g. Betz et al., 2008; Westneat et al., 2008) is a useful tool that makes it feasible to perform analyses of general mouthpart coordination in insects, including all mouthpart elements, and to aid in understanding the often complex kinematics of single mouthpart elements (e.g. of the maxillae).

In this study, we investigated how the biting and chewing mouthparts of the cockroach *P. americana* are mutually coordinated. Our hypotheses regarding their movement patterns with respect to their rhythmicity and stereotypy could be confirmed, even though it became clear that in certain mouthpart elements (depending on their functional role in the entire mouthpart complex) some degree of modulation is possible. This may help the animals to adjust to different feeding contexts, such as the mechanical properties of the food. Finally, our results of the movement analyses were used in combination with the morphological analyses to generate a two dimensional functional model of the movement cycle of the maxilla.

Kinematics of the mandibles

According to the hinge-like articulation of the mandibles to the head capsule, the opening angle of the mandibles (cf. angle *m* in Fig. 1 and Fig. 9B) is the only available parameter to describe mandibular kinematics (Fig. 1). In addition, the distance between both the mandibular apices (cf. ‘gap width of mandibles’ in Fig. 1 and Fig. 9B) during a movement cycle has been measured to elucidate the movement pattern of both mandibles simultaneously by means of a distance value. This parameter confines the maximum manageable size of a food bolus to approximately 740 µm (calculated grand mean over all 12 specimens).

The duration of an entire motion cycle of the mandibles amounts to 450–500 ms. This is in agreement with studies of Blaney and Chapman (Blaney and Chapman, 1970) in the locust *Schistocerca gregaria*, in which time intervals for motion cycles of the mandibles attain 270–550 ms. A strong rhythmicity of the mandibular movement was confirmed in our autocorrelation analysis (supplementary material Fig. S1A) supporting our hypothesis 1. In *Periplaneta*, the maxima and minima of the mandibular opening angles and the duration of a movement cycle show relatively low mean CVs (Fig. 4) across the 12 sequences, suggesting a rather stereotyped movement pattern (cf. hypothesis 1).

The angle versus time diagrams shown in Figs 1 and 2 depict similar patterns in the values of the rotation angles of both the left

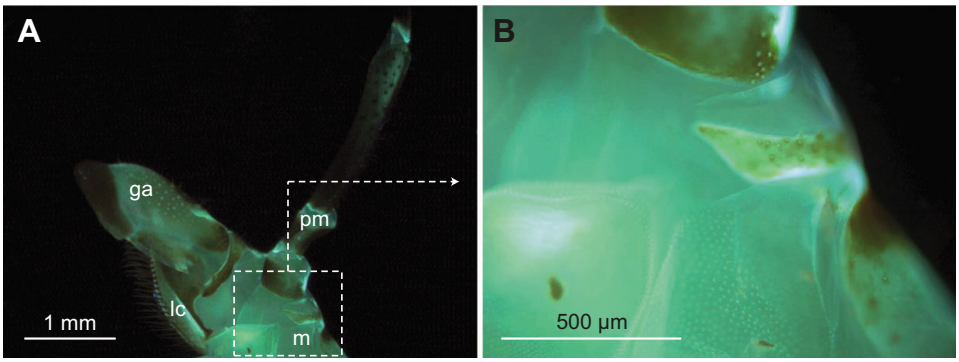

Fig. 7. Resilin distribution across the maxilla as established via fluorescence microscopy. (A) Overview of membranous surface area of the stipes (dorsal aspect of right maxilla) and (B) corresponding detailed view, showing cuticular areas with high levels of resilin inclusions in the cuticle. ga, galea; lc, lacinia; m, membranous surface area of the stipes; pm, palpus maxillaris/ maxillary palp.

and the right mandible regarding their temporal movement and their absolute values, a pattern that is representative for most of the analyzed sequences. This is further supported by the results of our correlation and principal component analyses (Fig. 3; Tables 1, 2) and indicates a bilateral coupling of both mandibles (cf. Popham, 1959; Popham, 1961) (cf. hypothesis 2).

As can be seen in Fig. 1, the time needed to open the mandibles is approximately as long as the time needed to close them, a trend that could be found in all 12 sequences. These results differ from the observations of Blaney and Chapman (Blaney and Chapman, 1970) and Seath (Seath, 1977a), who have determined, in *Schistocerca gregaria*, that the opening of the mandibles occurs twice as fast as the closing movement. Chapman (Chapman, 1995b) assumes that such differences might be attributable to the resistance of the food substrate during the closing movement of the mandibles. Hence, the pasty substrate with which the cockroaches were fed during our experiments might have enabled the observed fast closing movements.

Kinematics of the maxillae

We have used four angles (*a–d* in Fig. 10) to describe the movement of the cardo–stipes complex, and two angles (*e* and *f* in Fig. 10) for the description of the maxillary palp. In comparison with the mandibles, the movements of the multi-segmented maxillae exhibit a higher degree of freedom and are thus more complex. However, similar to the mandibles, we have determined high autocorrelation values regarding the rhythmicity of the angles of the maxillary body (supplementary material Fig. S1B–E) strengthening our hypothesis 1. In addition, only low overall variation of these angles (as indicated by CVs ≤10%) and strong correlations [high correlation coefficients (CC) indicate high levels of synchronicity] among these angles and between both body sides (Figs 3, 4; Tables 1, 2) were determined. The strong correlation among the angles *b*, *c* and *d* (Fig. 3; Tables 1, 2) can be explained, because all three angles are part of the same triangle. Our correlation and principal component analyses (Fig. 3; Tables 1, 2) suggest that the movement of just one component of the maxillary body influences the positions of all the other parts, being connected according to the principle of a multiple articulated chain (e.g. Nachtigall, 2005). For instance, in agreement with Kéler (Kéler, 1963), the protraction of the stipes is caused by the adduction of the cardo (Fig. 6: phase 4 to phase 1). Hence, an explanation of the kinematics of the maxillae requires the simultaneous monitoring of all its components, a condition fulfilled in our study.

As also confirmed by both our analyses (Fig. 3; Tables 1, 2) and our functional model of the maxillary movement (Fig. 6), the angles *a* and *d* run in antiphase (Fig. 9C,D, Fig. 10). That is, during the backward rotation of the cardo (causing the opening of the maxilla), the stipes is flexed inward, so that the galea and stipes can be held close to the medial head axis, keeping contact with the food bolus. Because neither of these movements mechanically implies each other, this can only be managed by a close coordination of the activity of the muscles M15, M17 and M18 (Table 3).

The maxillary palps are regularly moved back and forth (cf. Fig. 2C and Fig. 6A), whereas the maxima and minima of the oscillation angle *e* about the stipes is more variable compared with the other angles of the maxillary body (cf. Fig. 4A,B and supplementary material Fig. S1F). This view is further supported because both the palpus angles *e* and *f* tend to load on higher PCs in our PCA (cf. Table 2), as previously shown by Klein (Klein, 1982), who found only a loose coupling of the palps of crickets to the rhythmic feeding activities of the other mouthparts. Indeed, neural recordings of deafferented nerves of the SOG of the locust *Locusta migratoria* have revealed that the outputs of the motor neuron of a maxillary palpus muscle are only weakly coupled to the mandibular motor pattern (Rast and Bräunig, 2001a; Rast and Bräunig, 2001b). Moreover, the decreased rhythmic movements of the palps might be explained by their prevailing sensory function during feeding (cf. hypothesis 2).

According to Snodgrass (Snodgrass, 1993), the movements of the maxillae are effected by the action of 11 muscles (of which five muscles are exclusively connected with the maxillary palp). The single-segmented mandible can move only around one single axis of rotation, whereas the maxillary kinematics result from the interaction of both ab- and adductions toward the median axis and pro- and retractions directed back and forth (Popham, 1959; Popham, 1961). As depicted in our model of Fig. 6, one maxillary motion cycle consists of four consecutive phases describing the highly protracted condition of the maxillae (phase 1), the maximally retracted condition (phase 3) and both transition states in between (phases 2 and 4). Our functional model (Fig. 6) explains almost all of the observed maxillary movements by the operation of the powering muscles. However, the protraction of the maxillae (Fig. 6, phase 3 to phase 1) by the re-mobilization of the energy previously stored in the compression of the resilin-containing arthrodial membrane, which connects the cardo with the stipes. In addition, the opening of the angle *d* between the cardo and stipes enabling the maxillary protraction might be passively assisted by the pressure mutually exerted by both abutting galeae during the adduction process.

Based on our cineradiographic analyses [and in contrast to Popham (Popham, 1961), who assumed a hemolymph-driven process], we consider the mechanism behind the protraction of the maxillae (i.e. the transition between phases 3 and 1 in Fig. 6) to be a combination of muscle-effected and non-muscular (preflex) mechanisms caused by the elasticity of the arthrodial maxillary membranes. Around the joint of the cardo and stipes, we found significant autofluorescence upon excitation of these structures with UV light (Fig. 7), indicating the presence of the highly elastic protein resilin in the cuticle of this region. Acting in the described manner, the preflex mechanisms caused by the elastic arthrodial membranes might assist the action of the M17 in setting the process of protraction in motion just before the M17 starts to contract.

Kinematics of the labium

We have been able to quantify the pro- and retraction of the labium by means of distance versus time diagrams (Fig. 2D). As shown in this example, its kinematics could be rhythmic (cf. supplementary material Fig. S1H of our autocorrelation analysis) and consistent over the complete sequences, whereas in other sequences, these movements were less regular and might significantly differ in terms of both their temporal mode and amplitude, as indicated by their high CVs (Fig. 4) and their inconsistent pattern in the correlation analyses (Fig. 3) and the PCAs (cf. hypothesis 2). In accordance with this observation, Evans (Evans, 1964) characterizes the kinematics of the labium in carabid beetles as irregular and shows that the labium only retracts providing that a sufficient amount of food is located within the cibarium.

Coordination between mandibles, maxillae and labium

In chewing and biting insects, the food is generally assumed to be grasped by the maxillae, cut by the mandibles and further transported toward the mouth via the maxillae, the mandibles and the labium (e.g. Chapman, 1995a; Betz et al., 2003). From our functional model (Fig. 6), we can deduce that maxillary food

The Journal of Experimental Biology (2014) doi:10.1242/jeb.092742

transport is achieved during phases 2 and 3, in which the opened position of the maxillae might laterally grasp the food material to draw it backwards and, at the same time, prevent its lateral loss during mastication by the closing mandibles. These functions are probably further supported by the adductors of the galea and lacinia (cf. M19–M21 in Fig. 5 and Table 3) (cf. Popham, 1961). The labium prevents the food material from falling out ventrad. Its regular pro- and retraction movements support the other mouthparts in transporting the food toward the mouth and re-circulating it to the mandibles and maxillae. Popham (Popham, 1961) suggests that the final transport of the salivated food toward the pharynx is effected by suction initiated by the cibarial and esophageal dilator muscles. Indeed, such a mechanism is supported by our radiograms, showing that material is rapidly sucked into the foregut (cf. supplementary material Movie 1).

As is apparent from the angle versus time diagram in Fig. 2, the mandibular opening angle *m* and the maxillary angles *a* and *d* are, in most of the 12 examined sequences, significantly coordinated, which is confirmed by our correlation analyses (CCs ranging from −0.38 to −0.75; Fig. 3) and principal component statistics (Fig. 3; Tables 1, 2). When the opening angle of the mandibles increases (i.e. the mandibles are opening), the maxillary angle *d* also increases (i.e. the maxillae are protracting), whereas the value of the maxillary angle *a* decreases (i.e. the maxillae are adducting). Hence, the opening of the mandibles, the protraction and adduction of the maxillae are usually coordinated in an antiphasic manner over the course of time as previously stated for *P. americana* by Popham (Popham, 1961) (cf. hypotheses 1 and 2) [cf. also Evans (Evans, 1964) and Evans and Forsythe (Evans and Forsythe, 1985) for carabid beetles]. Such stereotyped coordination is generally presumed to be based on subesophageal pattern generators exhibiting fixed phase relationships in an intersegmental (i.e. between different neuromeres) and bilateral (i.e. between both body sides) coupling pattern (Rohrbacher, 1994a; Rohrbacher, 1994b; Rast and Bräunig, 2001a; Rast and Bräunig, 2001b). According to Rohrbacher (Rohrbacher, 1994a; Rohrbacher, 1994b), the observed coordination between the various pairs of mouthparts might be enabled by promotor SOG interneurons simultaneously functioning as local and intersegmental interneurons, which project over the neuromeral borders of the different mouthparts. According to their rhythmic activity patterns in relation to the chewing cycle, such modulatory interneurons are assumed to be associated with or part of a central pattern generator circuit for chewing (Rohrbacher, 1994b).

If the mean time needed for a motion cycle (grand mean over all sequences) is considered, the opening angle of the mandible *m* and both the maxillary angles *a* and *d* feature values between 446 and 498 ms. Moreover, in most of the analyzed sequences, the rotation of the maxillary palp around its basal articulation at the stipes is coordinated with the movements of the mandibles and the maxillae. This is reflected in the corresponding angle versus time diagram of the sequence *Periplaneta*_4 (Fig. 2), which is representative for most other sequences. The maxillary angle *e* (describing the rotation of the palp around its insertion) is correlated both with the opening angle of the mandibles (although the direction of the correlations is not uniform) and with the maxillary angle *d* (negative correlation in 10–11 of 12 sequences) (cf. Fig. 3). This means that while the maxilla is protracted, the maxillary palp is moved in a reverse (posterior) direction (abduction) (cf. Fig. 6).

The comparison of the distance versus time diagrams of the labial movement with the angle versus time diagrams of both mandibles and maxillae (mandibular opening angles *m* and maxillary angle *d*, respectively) shows that the protraction and retraction movements of the labium are coordinated with the opening of the mandibles and with the protraction of the maxillae in five of the 12 sequences analyzed by PCA. However, only weak coordination for three sequences and no coordination for three other sequences are observed with regard to the labium movement with the above-mentioned mandibular and maxillary angles. This finding is also supported by weak correlation coefficients (CC 0.33–0.46) and suggests that the neural coupling between these mouthparts is not as fixed as that found in mandibles and maxillae. Although the overall movements of the maxillary palp and the labium are coordinated with the kinematics of the mandibles and the maxillae, the variability of these mouthparts in terms of their minimal and maximal values and the time intervals necessary for a complete motion cycle are much higher than those observed for both mandibles and maxillae. This suggests a higher flexibility and context-dependent control of these components during the feeding process (cf. hypothesis 2).

MATERIALS AND METHODS

Animals

We examined adult American cockroaches (*P. americana*) of both sexes from our stock breeding. Animals were kept in large plastic boxes under constant temperature (29°C) and 40% relative humidity. A diurnal light–dark cycle of 12 h day:12 h night was chosen. Animals were fed with leaf salad, oatmeal and water *ad libitum*. All experiments were performed at room temperature (19–21°C).

Preparation of animals for *in vivo* radiography

Because the objective of this study was to describe exclusively the kinematics of the mouthparts, we needed to immobilize all the other extremities and the body of the cockroaches. To avoid unnecessary stress, the animals were tranquillized using CO_2. This treatment does not have an effect on the kinematics of the mouthparts as long as the cockroaches spend enough time in fresh air afterwards (Brooks, 1965; Nicolas and Sillans, 1989). The cockroaches were glued with their dorsal sides onto microscope slides using an instant adhesive. The leg extremities, the antennae and the neck were fixed with slender strips of adhesive tape. In order to analyze natural behaviour and to avoid long immobilization periods, preparation of the insects and *in vivo* radiography were synchronized as much as possible. The immobilized animals were then integrated into the experimental setup as depicted in Fig. 8. To stimulate the masticatory movements, a soft compound comprising homogenized diptera larvae, honey and some fish food flakes were applied into the region of the mouthparts using a pin head.

In vivo high-speed X-ray cineradiography

The experiments were performed at the ANKA (Angströmquelle Karlsruhe) synchrotron light source of the Karlsruhe Institute of Technology (KIT, Germany). The 2.5-GeV ANKA storage ring hosts the bending magnet beamline TopoTomo with its high resolution micro-imaging station. The photon flux density and spectral range of the TopoTomo source are well-suited for *in vivo* cineradiography. Details of the ANKA light source and the instrumentation of the TopoTomo beamline are available in Rack et al. (Rack et al., 2009) and Moser (Moser, 2001).

The experimental procedure was based on a protocol for fast *in vivo* X-ray imaging (frequently termed *in vivo* cineradiography), as published recently (Rack et al., 2010). In order to obtain the high data-acquisition rates required for *in vivo* cineradiography, TopoTomo was operated in the so-called white beam mode: only a 0.5 mm thick beryllium exit window and 1 mm thick silicon attenuation filter were placed between the light source and the experiment (Fig. 8). This results in a homogeneous wavefront profile, an integral photon flux density of 10^{10} Ph mm^{-2} s^{-1} and a mean energy around 20 keV at the position of the experiment. At 20 keV X-ray photon energy, the studied insects are almost transparent. Consequently, the negligible attenuation reduces the dose to the specimen. The contrast mode deployed for the presented results is related to the diffraction of the X-rays

The Journal of Experimental Biology (2014) doi:10.1242/jeb.092742

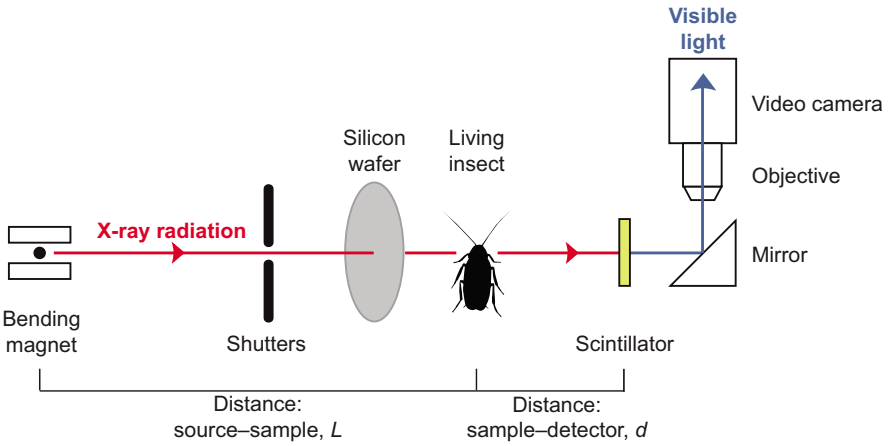

Fig. 8. Experimental setup for phase contrast *in vivo* cineradiography using synchrotron radiation at the TopoTomo beamline. The synchrotron radiation is generated by a bending magnet inside the storage ring, passes the various shutters, a beryllium exit window (not shown) and a silicon wafer, and permeates the head of the feeding cockroach. Subsequently, the X-rays are transformed into visible light by means of a scintillator. A visible light microscope with a folded beampath projects the luminescence image onto the chip of a high-speed camera in which the pictures are stored (figure modified from Westneat et al., 2008).

at the interfaces within the specimen, i.e. so-called inline X-ray phase contrast (Cloetens et al., 1996; Westneat et al., 2003; Betz et al., 2007; Socha et al., 2007; Westneat et al., 2008). Even though polychromatic radiation is used, the homogeneous wavefront profile of TopoTomo in the white-beam mode is excellently suited for phase contrast imaging (Weitkamp et al., 2011).

Further technical details of both our setup and the processing of the attained X-ray cineradiographic sequences are provided in the Appendix.

Processing and analyzing the X-ray cineradiographic sequences

In order to enhance the image quality within the sequences, each frame was corrected with reference images captured before cineradiography. The ImageJ (Schneider et al., 2012) plugin ANKAphase was used to perform this flat-field and dark-field correction (Weitkamp et al., 2011). Further adjustment of brightness and contrast values was performed using the picture processing software Adobe Photoshop (Adobe Systems, 2003).

Out of more than 50 cineradiographic sequences, a total number of 12 sequences representing 12 different individuals was chosen for further analyses by applying the following criteria: (1) the sequences had to show at least three complete motion cycles of the mouthparts; (2) the mouthparts of *P. americana* had to be located within the filmed visual range for at least three motion cycles, and the local resolution of the mouthparts had to display an acceptable quality; (3) if any movements of the head capsule occurred in addition to those of the mouthparts, the sequence was rejected; (4) the behaviour of the cockroach was not to be disturbed by the treatment or the high-energy radiation. In Table 4, a list of the chosen sequences and some additional information is depicted.

To be able to calculate angles that describe characteristic movement patterns during the mastication process, each frame of the X-ray sequences was digitized by setting landmarks to relevant morphological positions. For these landmarks, a point was defined by an *x*- and a *y*-coordinate and stored in a data matrix. This procedure was conducted with the software tpsUtil (Rohlf, 2004) and tpsDig2 (Rohlf, 2004). For each frame, 19 landmarks and in addition six fixed points (per sequence) were defined to mark the corners of the triangles (an overview and a list of these landmarks and the corresponding structures are given in Fig. 9A and Tables 5, 6, respectively). The coordinates of the landmarks were afterwards exported to Microsoft Excel (Microsoft Corporation, 2003) to calculate triangles using basic trigonometric functions (calculation of distances between landmarks; calculation of angles by using the law of cosine). Changes in given angles within the movie revealed information about changes in the position of defined morphological structures and thus information about the kinematics of the individual mouthpart elements. For further analyses, selected landmarks were connected by straight lines to form triangles (Fig. 9B–E, Fig. 10).

Further details on the calculation of the relevant angles and distances for the different mouthparts are provided in the Appendix.

Table 4. List of the 12 selected radiographic sequences (movies) with information about the number of analyzed motion cycles of the mouthparts, the temporal resolution and the length of the sequences indicated by the total number of frames

Name of movie	Σ motion cycles	Image acquisition rate (fps)	Sequence length (Σ frames)
*Periplaneta*_1	8	60	247
*Periplaneta*_2	5	60	99
*Periplaneta*_3	7	60	200
*Periplaneta*_4	6	60	172
*Periplaneta*_5	5	60	160
*Periplaneta*_6	3	125	196
*Periplaneta*_7	4	125	232
*Periplaneta*_8	12	60	211
*Periplaneta*_9	4	125	283
*Periplaneta*_10	7	125	342
*Periplaneta*_11	4	125	259
*Periplaneta*_12	3	125	254

Generation of angle–time diagrams

For each single frame of a movie, the angles described in Figs 9 and 10 were calculated. The temporal sampling rate (fps) that was applied and the exposure time per frame amounted to 16.67 ms (60 fps) and 8 ms (125 fps), respectively. This information was used to generate angle versus time diagrams.

Statistical analyses

To analyze the variability of the various mouthpart components in their local and temporal course of motion, the grand means (corresponding to the mean of the arithmetic means) of the maximum and minimum values of all the angles shown in Figs 9 and 10 and the time span necessary for a complete motion cycle were calculated. The grand means were based on the arithmetic means of the 12 cockroach specimens as calculated from 3 to 12 single motion cycles (cf. Table 4). In order to evaluate the overall variability of the individual angles and time courses, we calculated boxplots summarizing the medians and variation of the 12 coefficients of variation as calculated for each specimen (Fig. 4).

The interdependence between the movement patterns of the various mouthpart components was analyzed by correlation analyses. To this end, for each of the 12 specimens, we analyzed the correlations of all the measured angles and distances on a frame-by-frame basis and summarized the number of established significant positive and negative correlations in a table (Fig. 3).

A principal component analysis (PCA) was performed for each of the 12 specimens to obtain information about the extent of coordination between the various mouthpart elements. In total, 16 variables [i.e. the angles *a*–*f* and *m* of both body sides and the distance values (gap width of mandibles and protraction distances of labium)] were considered in the analysis, whereby 99–342 cases (=succeeding frames of each sequence) were analyzed. We used the Varimax option with Kaiser Normalization; all PCs with eigenvalues >1 were extracted, and all the variables with correlation

The Journal of Experimental Biology (2014) doi:10.1242/jeb.092742

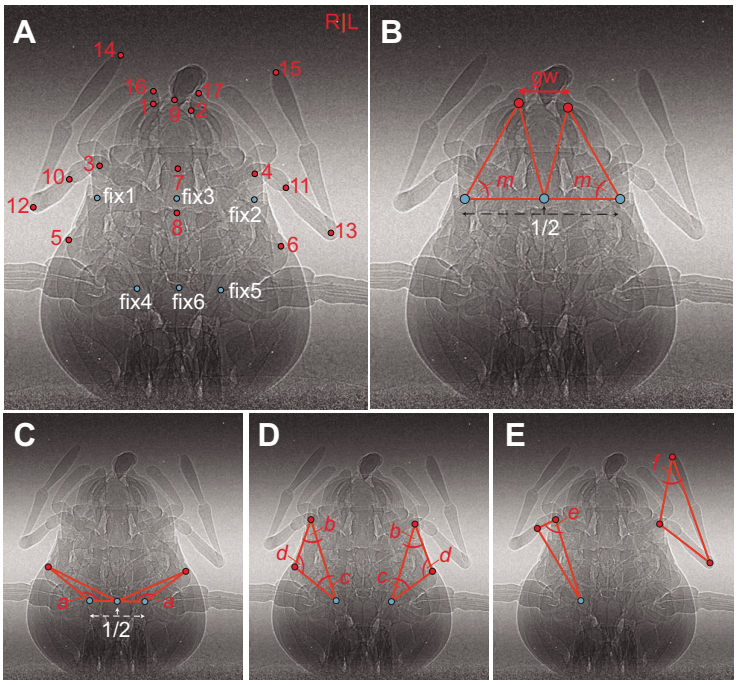

Fig. 9. Ventral views of the radiographic image of the head of *P. americana*. (A) Indication of the 19 moving landmarks (red dots) and the six fixed landmarks (blue dots). Both denote important morphological structures that are important for the kinematic analyses. (B) Construction of the triangles used to calculate the mandibular opening angle *m* and definition of the 'gap width of mandibles'. (C–E) Construction of the triangles used to calculate the respective maxillary angles. Red points are movable in their positions, blue points indicate fixed points. (C) Angle *a* is characteristic for the abduction and the adduction movement of the cardo. (D) Angle *b* indicates the degree of protraction of the complete maxilla; angles *c* and *d* depict the bending between cardo and stipes corresponding to the degree of maxillary pro- or retraction. (E) Angles *e* and *f* are indicators for the kinematics of the palpomeres of the maxillary palp. gw, gap width; R|L, right|left. For explanations of the landmarks see Tables 5 and 6.

coefficients <–0.5 and >0.5 were chosen for the interpretation of the extracted PCs.

The correlation coefficients that exhibited statistical significance were used as a measure of how strongly two mouthpart elements move in a coordinate pattern. To assess the degree of coordination, we used the conventional interpretation of the correlation coefficient (CC) (Bühl, 2008). A missing or only weak coordination (CC 0–0.5) is indicative of a high modulation capacity, whereas a high or very high coordination (CC 0.7–1) represents a strong stereotypy of the movements. Correlation coefficients in the intermediate range (CC 0.5–0.7) indicate a medium coordination. Finally, to assess a rhythmical behaviour within a given time series (i.e. the pattern of the values of an angle over time), we performed autocorrelation analyses (e.g. Hammer and Harper, 2006) for the various angles of the kinematic sequence *Periplaneta*_4 (cf. Figs 1, 2). This sequence is representative for almost all other sequences analyzed in this study. The autocorrelation analyses were performed with the software PAST (version: 3.0) (Hammer et al., 2001), whereas the software SPSS 16 (SPSS Inc., 2007) was used for all other statistical calculations.

Table 5. Description of the movable landmarks displayed in Fig. 9, indicating the respective morphological structures

Labels of landmarks	Morphological structures
1	Tip of mandible right
2	Tip of mandible left
3	Insertion of maxillary palp at stipes right
4	Insertion of maxillary palp at stipes left
5	Articulation between cardo and stipes right
6	Articulation between cardo and stipes left
7	Front edge of prementum
8	Front edge of mentum
9	Front edge of labrum
10	End 1st palpomere of maxillary palp right
11	End 1st palpomere of maxillary palp left
12	End 2nd palpomere of maxillary palp right
13	End 2nd palpomere of maxillary palp left
14	End 4th palpomere of maxillary palp right
15	End 4th palpomere of maxillary palp left
16	Tip of maxilla (galea) right
17	Tip of maxilla (galea) left

Generation of a two-dimensional functional model for maxillary kinematics

The observed complex kinematics of the maxillae was illustrated in the form of a two-dimensional functional model to demonstrate the true-to-scale position of the maxilla and its muscles during the various phases of the movement cycle. The size ratios of the various maxillary components, the location of the muscles and their articulation points (*origo* and *insertio*) were elucidated by scanning electron microscopy (SEM) studies, dissections of the maxillae and additional data from the literature (Weber, 1933; Snodgrass, 1950; Snodgrass, 1951; Kéler, 1963; Matsuda, 1965; Snodgrass, 1993). The angular shifts of the maxillary components over time in the functional model strictly followed the observed angular measurements in the *in vivo* cineradiography. Our schematic model elucidates the hypothetical general effect that each maxillary muscle has on the observed overall maxillary movement pattern. It neither aims at reflecting the actual activity pattern of these muscles as deducible from electrophysiological studies, nor does it quantitatively model the possibly involved multiple bar linkage as applied to fish jaws by Westneat (Westneat, 1994; Westneat, 2003). However, our model forms a starting point for such kinds of physiological and biomechanical analyses.

SEM preparation was performed according to standard procedures (i.e. critical point drying followed by sputter coating) as described previously (Betz et al., 2003).

The presence and distribution of the elastic protein resilin in the maxillary cuticle of *P. americana* was analyzed by means of fluorescence microscopy. According to Gorb (Gorb, 1999), Neff et al. (Neff et al., 2000) and Haas et al. (Haas et al., 2000), the insect cuticle exhibits a pronounced autofluorescence in the wavelength range of blue-green to red-infrared.

Table 6. Description of the fixed landmarks displayed in Fig. 9 indicating the respective morphological structures.

Labels of fixed landmarks	Morphological structures
Fix1	Pivot point of the left mandible
Fix2	Pivot point of the right mandible
Fix3	Center between fix1 and fix2
Fix4	Pivot point of the cardo of the left maxilla
Fix5	Pivot point of the cardo of the right maxilla
Fix6	Center between fix4 and fix5

The Journal of Experimental Biology (2014) doi:10.1242/jeb.092742

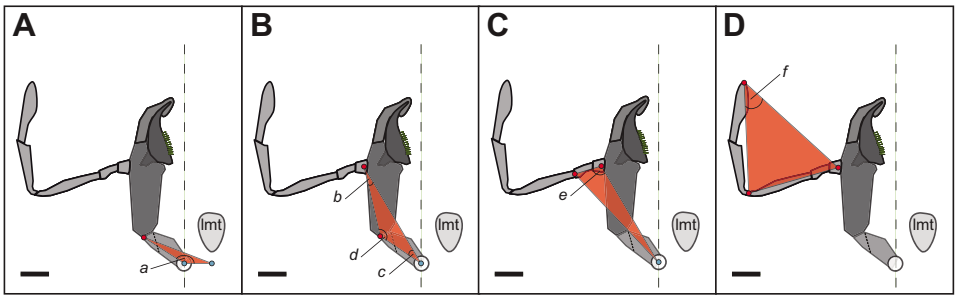

Fig. 10. Model of the maxilla, highlighting the triangles used to calculate the various maxillary angles. Red points are movable in their positions, blue points indicate fixed points. For an explanation of angles *a–f*, see Fig. 9. lmt, laminatentorium. Scale bars: 1 mm.

However, as soon as the cuticle is excited with light within the narrow band of 330–380 nm (UV light), all cuticle areas containing resilin emit blue light (approximately 420 nm) (Edwards, 1983; Gorb, 1999). For fluorescence microscopy, the mouthparts of freshly killed cockroaches were placed onto hollow slides with distilled water. The obtained preparation was examined at various wavelength ranges (all UV light) with a fluorescence microscope (Leica DM5000 D and Leica CTR 5000, Wetzlar, Germany) and digitally captured with the attached camera (Leica DFC 320, Wetzlar, Germany).

APPENDIX

Technical setup of applied *in vivo* high-speed X-ray cineradiography

In order to fully exploit the benefits of phase-sensitive X-ray imaging, the required detector (a so-called macroscope) was placed 0.5 m downstream of the specimen. Its acquisition scheme was based on the indirect concept whereby the luminescence image of a scintillator is captured by a camera via visible light optics. For the macroscope, two Rodenstock objectives (1.5× and 3.6×) in combination with a commercial tele-objective were combined to reach a high visible light throughput, while preserving a large field of view with low magnifications. Bulk single-crystal $CdWO_4$ (CWO) and Ce-doped $(LuY)_2SiO_2$ (LYSO:Ce) were used as a luminescence screen. In an ideal case, the choice of the scintillator is driven by its stopping power, light yield and response time that are, in our case, predetermined by the time-resolved nature of the study. Nevertheless, technical feasibilities such as the availability of a given thickness in optically polished quality also have to be considered. Hence, LYSO:Ce is well suited for our purposes as it is fast, has both a high stopping power and light yield, even though it was only available as crystals with a thickness of several 100 µm. For higher resolutions, we therefore needed to switch to CWO, which was available as much thinner crystal. The magnified visible light image of the scintillator crystal was recorded by a commercial CMOS-based camera: Photron SA1 (1024 × 1024 pixels, 20 µm pixel size, up to 5400 full-images s^{-1} data acquisition rate, 42% peak quantum efficiency at 640 nm, 10 bit (800:1) dynamic range with a 12 bit digitalization) (Rack et al., 2009; Rack et al., 2010).

To reduce the radiation dose to the specimens further, pre-alignment of the cockroach heads with respect to the field of view of the detector was performed with visible light. To survey the correct alignment, a theodolite was used; its focal plane was set to overlap with the field of view of the detector with respect to the X-ray beam. For recording a sequence of images (frequently termed movie), the Photron SA1 was operated in the so-called ring buffer mode (i.e. the camera was in continuous recording mode; once the camera memory was filled, the recorded data was overwritten by newly incoming data starting at the beginning of the memory). The fast shutter available at TopoTomo allowed dead times to be reduced still further, so that the specimen was only exposed to radiation when movies were recorded.

Synchrotron inline phase-contrast is a well-known approach to reduce the radiation dose applied to the sample. Because the absorption of the sample is reduced while the refraction at the interfaces is exploited as contrast, it is possible to perform *in vivo* experiments. However, the settings available at the TopoTomo beamline in terms of flux for a given X-ray wavelength do not allow *in vivo* studies over an extended period of time. Usually after a few seconds of synchrotron irradiation, a striking change in behaviour was observed in the experimental animals. This was characterized by significantly decelerated movements and was sometimes accompanied by the swallowing of air. A further criterion for a natural footage sequence was a continuous flow of the feeding stream through the foregut that was only visible for a few seconds upon synchrotron irradiation. Therefore, to ensure that most natural behaviours were analyzed in this study, only the sequences occurring immediately after the onset of the beam and broadly before the onset of the described artificial behaviour were analyzed.

Calculation of triangles using basic trigonometric functions for the description of the kinematics of the different mouthparts

Mandibles

For the characterization of the opening and closing movements of the mandibles, a triangle was constructed that connected the tip of the mandibles, their pivot points and a theoretical point situated in the middle between the pivot points of the left and the right side (Fig. 9B). The opening-angle *m* of the mandibles described the rotation of the mandible within the rotation axis of the dicondylic articulation. The distance between the tips of both the mandibles was defined as the ‘gap width of mandibles’.

Maxillae

Owing to the complexity of the maxillae, a series of different triangles with several angles had to be constructed that described both the abduction and the adduction of the cardo (angle *a*), the protraction of the complete maxilla (angle *b*) and the bending between the cardo and the stipes corresponding to the pro- and retraction of the maxilla (angles *c* and *d*). Furthermore, triangles were constructed to quantify the kinematics within the palpomeres of the maxillary palps (angles *e* and *f*). The construction concept of the relevant triangles and the models of the maxillary angles are depicted in Fig. 9C–E and Fig. 10.

Labium

In order to describe the forward and backward movements of the labium, the positions of the front edges of the prementum (landmark 7) and the mentum (landmark 8) (Fig. 9A) were determined over time. For each frame, the distance between the actual position and the most retracted condition was defined with a metric value.

Acknowledgements
This paper is dedicated to the entomologist Prof. Dr Thomas Bauer (University of Kiel, Germany) on the occasion of his 70th birthday. We thank Wah-Keat Lee (Brookhaven National Labs) and Mark Westneat (Field Museum of Natural History, Chicago) for their suggestion for this work. We acknowledge the Synchrotron Light Source ANKA for provision of beamtime at the TopoTomo beamline. We wish to thank L. Koerner, A. Dieterich, A. Ershov, K.-H. Hellmer and M. Meinert for technical assistance; D. Haas for providing the ImageJ plugin ANKAphase; and A. Schmitt for proofreading the manuscript.

Competing interests
The authors declare no competing financial interests.

Author contributions
The work presented here was carried out in collaboration between all authors. C.S. and O.B. defined the research theme. AR was responsible for the experimental beamline setup and the corresponding material and method section. All authors recorded the data at TopoTomo beamline. C.S., analysed the data, interpreted the results and wrote the paper. O.B. supervised this work. All authors have contributed to, seen and approved the manuscript.

Funding
O.B. and C.S. received financial support from the Deutsche Forschungsgemeinschaft (DFG) [BE-2233/6-3].

Supplementary material
Supplementary material available online at
http://jeb.biologists.org/lookup/suppl/doi:10.1242/jeb.092742/-/DC1

References

Altman, J. S. and Kien, J. (1979). Suboesophageal neurons involved in head movements and feeding in locusts. *Proc. R. Soc. B* **205**, 209-227.
Betz, O., Newton, A. F. and Thayer, M. K. (2003). Comparative morphology and evolutionary pathways of the mouthparts of spore-feeding Staphylinoidea (Coleoptera). *Acta Zool.* **84**, 179-238.
Betz, O., Wegst, U., Weide, D., Heethoff, M., Helfen, L., Lee, W.-K. and Cloetens, P. (2007). Imaging applications of synchrotron X-ray phase-contrast microtomography in biological morphology and biomaterials science. I. General aspects of the technique and its advantages in the analysis of millimetre-sized arthropod structure. *J. Microsc.* **227**, 51-71.
Betz, O., Rack, A., Schmitt, C., Ershov, A., Dieterich, A., Körner, L., Haas, D. and Baumbach, T. (2008). High-speed X-ray cineradiography for analyzing complex kinematics in living insects. *Synchrotron Radiat. News* **21**, 34-38.
Blaney, W. M. and Chapman, R. F. (1970). The functions of the maxillary palps of Acrididae (Orthoptera). *Entomol. Exp. Appl.* **13**, 363-376.
Blaney, W. M. and Simmonds, M. S. J. (1987). Control of mouthparts by the subesophageal ganglion. In *Arthropod Brain: its Evolution, Development, Structure and Functions* (ed. A. P. Gupta), pp. 303-322. New York, NY: Wiley.
Brooks, M. A. (1965). The effects of repeated anesthesia on the biology of *Blattella germanica* (Linnaeus). *Entomol. Exp. Appl.* **8**, 39-48.
Bühl, A. (2008). *SPSS 16. Einführung in die moderne Datenanalyse*, pp. 346. München: Pearson Education.
Chapman, R. F. (1995a). Mechanics of food handling by chewing insects. In *Regulatory Mechanisms in Insect Feeding* (ed. R. F. Chapman and G. de Boer), pp. 3-31. New York, NY: Chapman & Hall.
Chapman, R. F. (1995b). Chemosensory regulation of feeding. In *Regulatory Mechanisms in Insect Feeding* (ed. R. F. Chapman and G. de Boer), pp. 101-136. New York, NY: Chapman & Hall.
Cloetens, P., Barrett, R., Baruchel, J., Guigay, J.-P. and Schlenker, M. (1996). Phase objects in synchrotron radiation hard X-ray imaging. *J. Phys. D: Appl. Phys.* **29**, 133-146.
Edwards, H. A. (1983). Occurrence of resilin in elastic structures in the food-pump of reduviid bugs. *J. Exp. Biol.* **105**, 407-409.
Evans, M. E. G. (1964). A comparative account of the feeding methods of the beetles *Nebria brevicollis* (F.) (Carabidae) and *Philonthus decorus* (Grav.) (Staphylinidae). *Trans. R. Soc. Edinb.* **66**, 91-109.
Evans, M. E. G. and Forsythe, T. G. (1985). Feeding mechanisms, and their variation in form, of some adult ground-beetles (Coleoptera: Caraboidea). *J. Zool.* **206**, 113-143.
Forsythe, T. G. (1982). Feeding mechanisms of certain ground beetles (Coleoptera: Carabidae). *Coleopts Bull.* **36**, 26-73.
Forsythe, T. G. (1983). Mouthparts and feeding of certain ground beetles (Coleoptera: Carabidae). *Zool. J. Linn. Soc.* **79**, 319-376.
Gorb, S. N. (1999). Serial elastic elements in the damselfly wing: mobile vein joints contain resilin. *Naturwissenschaften* **86**, 552-555.
Griss, C. (1990). Mandibular motor neurons of the caterpillar of the hawk moth *Manduca sexta*. *J. Comp. Neurol.* **296**, 393-402.
Griss, C., Simpson, S. J., Rohrbacher, J. and Rowell, C. H. F. (1991). Localization in the central nervous system of larval *Manduca sexta* (Lepidoptera: Sphingidae) of areas responsible for aspects of feeding behaviour. *J. Insect Physiol.* **37**, 477-482.
Haas, F., Gorb, S. and Wootton, R. J. (2000). Elastic joints in dermapteran hind wings: materials and wing folding. *Arthropod Struct. Dev.* **29**, 137-146.
Hammer, Ø. and Harper, D. A. T. (2006). *Paleontological Data Analysis*, 1st edn. Oxford: Blackwell Publishing.
Hammer, Ø., Harper, D. A. T. and Ryan, P. D. (2001). PAST: paleontological statistics software package for education and data analysis. *Palaeontological Association* **4**, 1-9.
Kéler, S. v. (1963). *Entomologisches Wörterbuch mit besonderer Berücksichtigung der morphologischen Terminologie*. Berlin: Akademie-Verlag.
Kent, K. S. and Hildebrand, J. G. (1987). Cephalic sensory pathways in the central nervous system of larval *Manduca sexta* (Lepidoptera: Sphingidae). *Philos. Trans. R. Soc. B* **315**, 1-36.
Klein, U. (1982). The articulation of cricket palps: morphology and movement pattern in behaviour. *Physiol. Entomol.* **7**, 297-314.
Matsuda, R. (1965). Morphology and evolution of the insect head. *Mem. Am. Entomol. Inst.* **4**, 1-334.
Moser, H. O. (2001). New synchrotron radiation facility ANKA at Karlsruhe. *J. Alloy. Comp.* **328**, 42-49.
Nachtigall, W. (2005). *Biologisches Design: Systematischer Katalog der Bionik für Designer, Konstrukteure und Biowissenschaftler*. Berlin: Springer.
Neff, D., Frazier, S. F., Quimby, L., Wang, R. T. and Zill, S. (2000). Identification of resilin in the leg of cockroach, *Periplaneta americana*: confirmation by a simple method using pH dependence of UV fluorescence. *Arthropod Struct. Dev.* **29**, 75-83.
Nicolas, G. and Sillans, D. (1989). Immediate and latent effects of carbon dioxide on insects. *Annu. Rev. Entomol.* **34**, 97-116.
Popham, E. J. (1959). The anatomy in relation to feeding habits of *Forficula auricularia* L. and other Dermaptera. *Proc. Zool. Soc. Lond.* **133**, 251-300.
Popham, E. J. (1961). The functional morphology of the mouthparts of the cockroach *Periplaneta americana* L. *Entomologist.* **94**, 185-192.
Rack, A., Weitkamp, T., Bauer Trabelsi, S., Modregger, P., Cecilia, A., dos Santos Rolo, T., Rack, T., Haas, D., Simon, R., Heldele, R. et al. (2009). The micro-imaging station of the TopoTomo beamline at the ANKA synchrotron light source. *Nucl. Instrum. Methods Phys. Res. B* **267**, 1978-1988.
Rack, A., Garcia-Moreno, F., Schmitt, C., Betz, O., Cecilia, A., Ershov, A., Rack, T., Banhart, J. and Zabler, S. (2010). On the possibilities of hard X-ray imaging with high spatio-temporal resolution using polychromatic synchrotron radiation. *J. XRay Sci. Technol.* **18**, 429-441.
Rast, G. F. and Bräunig, P. (2001a). Feeding-related motor patterns of the locust suboesophageal ganglion induced by pilocarpine and IBMX. *J. Insect Physiol.* **47**, 43-53.
Rast, G. F. and Bräunig, P. (2001b). Insect mouthpart motor patterns: central circuits modified for highly derived appendages? *Neuroscience* **108**, 167-176.
Rohlf, F. J. (2004). TPSDig2: A program for landmark development and analysis. Stony Brook, NY: State University of New York. Available at: http://life.bio.sunysb.edu/morph/
Rohrbacher, J. (1994a). Mandibular premotor interneurons of larval *Manduca sexta*. *J. Comp. Physiol.* **175**, 619-628.
Rohrbacher, J. (1994b). Fictive chewing activity in motor neurons and interneurons of the suboesophageal gangion of *Manduca sexta* larvae. *J. Comp. Physiol.* **175**, 629-637.
Schmitt, C., Rack, A., Koerner, L., Dieterich, A., Zabler, S. and Betz, O. (2009). High-speed cineradiography for imaging the mouthpart kinematics of living insects. *ANKA Highlights.* **2009**, 25-26.
Schneider, C. A., Rasband, W. S. and Eliceiri, K. W. (2012). NIH Image to ImageJ: 25 years of image analysis. *Nat. Methods* **9**, 671-675.
Seath, I. (1977a). Sensory feedback in the control of mouthpart movements in the desert locust *Schistocerca gregaria*. *Physiol. Entomol.* **2**, 147-156.
Seath, I. (1977b). The effects of increasing mandibular load on electrical activity in the mandibular closer muscles during feeding in the desert locust, *Schistocerca gregaria*. *Physiol. Entomol.* **2**, 237-240.
Smith, J. J. B. (1985). Feeding mechanisms. In *Comprehensive Insect Physiology, Biochemistry and Pharmacology* (ed. G. A. Kerkut and L. I. Gilbert), pp. 33-36. Oxford: Pergamon Press.
Snodgrass, R. E. (1950). Comparative studies on the jaws of mandibulate arthropods. *Smithsonian Miscellaneous Collection* **116**, 1-85.
Snodgrass, R. E. (1951). *Comparative Studies on the Head of Mandibulate Arthropods*. Ithaca, NY: Comstock Publishing Company, Inc.
Snodgrass, R. E. (1993). *Principles of Insect Morphology* – with a new foreword by George C. Eickwort. Ithaca, NY: Cornell University Press.
Socha, J. J., Westneat, M. W., Harrison, J. F., Waters, J. S. and Lee, W.-K. (2007). Real-time phase-contrast x-ray imaging: a new technique for the study of animal form and function. *BMC Biol.* **5**, 6.
Weber, H. (1933). *Lehrbuch der Entomologie*. Jena: Gustav Fischer Verlag.
Weitkamp, T., Haas, D., Wegrzynek, D. and Rack, A. (2011). ANKAphase: software for single-distance phase retrieval from inline X-ray phase-contrast radiographs. *J. Synchrotron Radiat.* **18**, 617-629.
Westneat, M. W. (1994). Transmission of force and velocity in the feeding mechanisms of labrid fishes (Teleostei, Perciformes). *Zoomorphology* **114**, 103-118.
Westneat, M. W. (2003). A biomechanical model for analysis of muscle force, power output and lower jaw motion in fishes. *J. Theor. Biol.* **223**, 269-281.
Westneat, M. W., Betz, O., Blob, R. W., Fezzaa, K., Cooper, W. J. and Lee, W.-K. (2003). Tracheal respiration in insects visualized with synchrotron x-ray imaging. *Science* **299**, 558-560.
Westneat, M. W., Socha, J. J. and Lee, W.-K. (2008). Advances in biological structure, function, and physiology using synchrotron X-ray imaging. *Annu. Rev. Physiol.* **70**, 119-142.

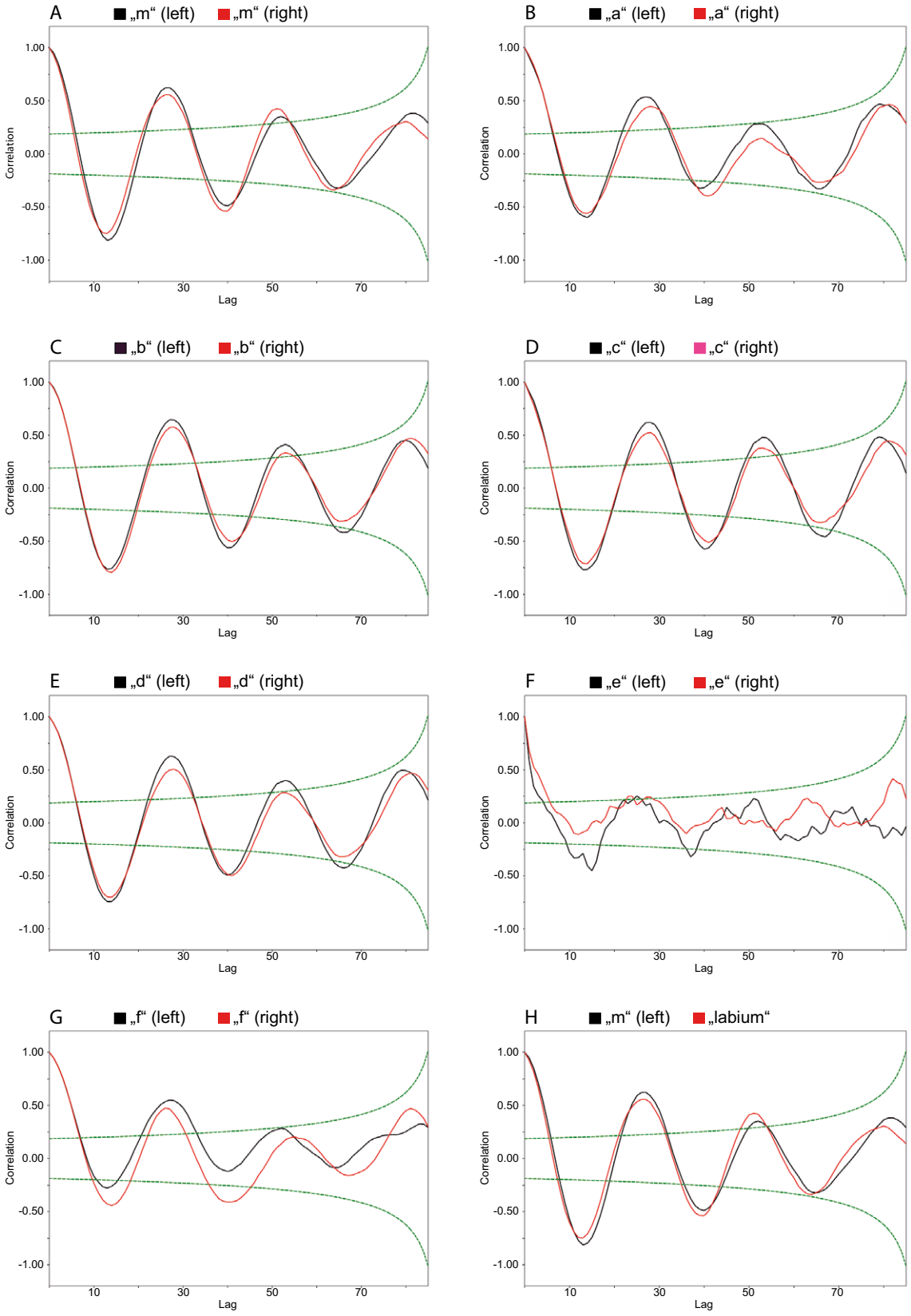

Fig. S1. Autocorrelation diagrams (i.e. autocorrelation coefficients versus lag time) for the representative sequence “*Periplaneta*_4” as shown in Figs 1 and 10 of the main text. For an explanation of angles “m” and “a”-“f”, see Fig. 10 of the main text. “Labium” refers to the pro- and retraction movements of the labium. The dashed lines indicate the 95% confidence intervals of the autocorrelation coefficients displayed on the *y*-axis. Where these are intersected by the autocorrelation curves, the autocorrelations are statistically significant. The black and red curves are indicative of the respective left and right mouthparts, showing their degree of synchronicity. Only the movement of the labium (H) is shown in concert with that of the left mandible.

Movie 1.

Movie 2.

Movies 1 and 2. Synchrotron-based X-ray cineradiographic movie sequences showing all mouthpart elements interacting during food uptake in our model system *Periplaneta americana*.